DMCMN: Experimental/Analytical Evaluation of the Effect of Tip Mass on Atomic Force Microscope Cantilever Calibration

Matthew S. Allen[*], Hartono Sumali[§] & Peter C. Penegor[+]

[*]Assistant Professor, University of Wisconsin-Madison, 535 ERB, 1500 Engineering Drive, Madison, WI 53706,

Corresponding Author: msallen@engr.wisc.edu

[§]Principal Member of Technical Staff, Sandia National Laboratories[1] P.O. Box 5800, Albuquerque, NM 87185,

hsumali@sandia.gov

[+]Undergraduate Student, University of Wisconsin-Madison

Abstract:

Quantitative studies of material properties and interfaces using the Atomic Force Microscope (AFM) have important applications in engineering, biotechnology and chemistry. Contrary to what the name suggests, the AFM actually measures the displacement of a micro-scale probe, so one must determine the stiffness of the probe to find the force exerted on a sample. Numerous methods have been proposed for determining the spring constant of AFM cantilever probes, yet most neglect the mass of the probe tip. This work explores the effect of the tip mass on AFM calibration using the method of Sader and extends that method to account for a massive, rigid tip. One can use this modified method to estimate the spring constant of a cantilever from the measured natural frequency and Q-factor for any mode of the probe. This may be helpful when the fundamental mode is difficult to measure or to check for inaccuracies in the calibration obtained with the fundamental mode. The error analysis presented here shows that if the tip is not considered, then the error in the static stiffness is of roughly of the same order as the ratio of the tip's mass to the cantilever beam's. The area density of the AFM probe is also

[1] Sandia is a multiprogram laboratory operated by Sandia Corporation, a Lockheed Martin Company, for the United States Department of Energy's National Nuclear Security Administration under Contract DE-AC04-94AL85000.

misestimated if the tip mass is not accounted for, although the trends are different. The model presented here can be used to identify the mass of a probe tip from measurements of the natural frequencies of the probe. These concepts are applied to six low-spring constant, contact-mode AFM cantilevers, and the results suggest that some of the probes are well modeled by an Euler-Bernoulli beam with a constant cross section and a rigid tip, while others are not. One probe is examined in detail, using scanning electron microscopy to quantify the size of the tip and the thickness uniformity of the probe, and Laser Doppler vibrometry is used to measure the first four mode shapes. The results suggest that this probe's thickness is significantly non-uniform, so the models upon which dynamic calibration is based may not be appropriate for this probe.

1. Introduction

The Atomic Force Microscope (AFM) has long since proven its utility for imaging at very small scales [1]. In recent years, there has been considerable effort to obtain quantitative information regarding material properties, friction and wear at the nanoscale using the AFM. To make quantitative measurements, one must determine the spring constant of the cantilever to compute the force that the probe exerts on a sample for a measured deflection. This allows one to determine the force exerted on a sample during contact mode imaging, which is needed, for example, when studying the friction and wear properties of surfaces [2]. The force is also of interest when studying the strengths of bonds and the associated interaction forces [3-5], and recent works have shown that AFM measurements of cell stiffness can be used to discern cancer cells from healthy cells in some situations where traditional tests may fail [6, 7].

A number of procedures have been proposed to find the stiffness of AFM cantilevers [8-13]. Static methods have been developed, such as the method by Tortonese and Kirk which computes the stiffness of a cantilever by deflecting a reference lever of known stiffness [12], yet there are a number of limitations such as uncertainty due to friction and alignment [14], the potential for damaging or contaminating the tip during calibration and the need to calibrate the reference cantilever as well. This work focuses on the Sader calibration method [9], which uses an analytical model for the interaction of the cantilever with the surrounding fluid to solve for the unknown density per unit area and stiffness of the cantilever from measurements of its resonance frequency and Q-factor in the fluid. Two other common methods are the thermal method of Hutter & Bechhoefer [10] (also see [15-18] and their references for important corrections), and the Cleveland method [11, 13]. The thermal method utilizes the equipartition theorem to find the cantilever's spring constant from the magnitude of its mean-square

thermal vibration in air or in vacuum. The Cleveland method involves attaching nanoscale beads with known mass to the cantilever and uses the shift in the resonance frequencies to determine the spring constant. The thermal and Sader methods have recently been combined [19] to allow one to calibrate the stiffness and deflection sensitivity of AFM probes without bringing the probe in contact with a surface, which may damage delicate tips. Some of these dynamic methods have been compared in a few works [17, 20-22], generally showing good agreement so long as certain factors are correctly accounted for, such as the laser spot size in the thermal method [18]. Many of these methods have also been extended to calibrate the torsional stiffness of cantilevers [23], although this subject will not be treated here.

The dynamic calibration methods cited above rely on an analytical model for the probe, typically an Euler-Bernoulli beam model, and they do not explicitly consider the probe tip. One exception is the Cleveland method [13], which could be readily extended to treat a cantilever with a tip of known mass, although most available methods for estimating the mass of the probe tip, such as SEM imaging, are cumbersome. The authors are not aware of a work that has quantified the error that would be incurred in the Sader method due to the neglected tip. There is reason for concern because the tip is almost as massive as the cantilever for a number of commercially available probes, especially the thin, flexible cantilevers that are used for some of the most sensitive force measurements and the very small cantilevers that are used to acquire tapping-mode images at very high speeds [24]. For example, Figure 1 shows a Scanning Electron Microscope (SEM) image of one of the probes studied here, which shows that the tip volume is clearly significant relative to that of the beam. One should also recall that mass added to the tip of a cantilever can have a much larger dynamic effect than if the same mass were distributed along the length of the cantilever [25].

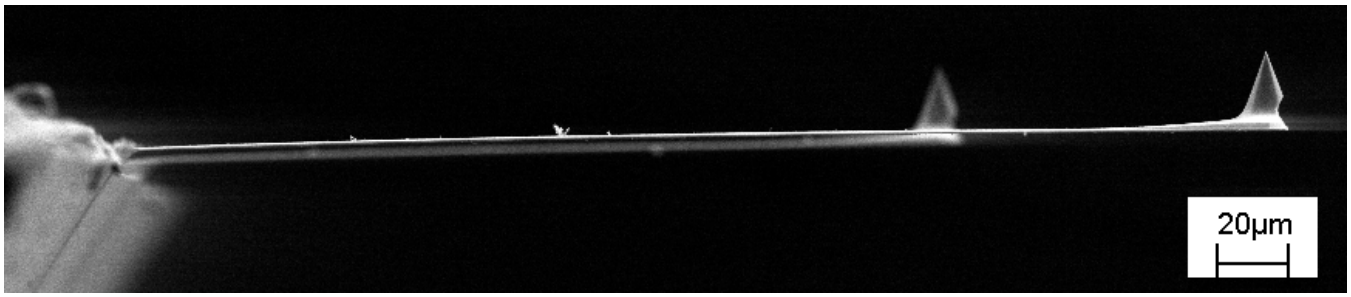

Figure 1: SEM image of a CSC38-B cantilever, similar to the one discussed in Section 3. The shorter cantilever in the background is a CSC38-A cantilever, which is mounted on the same chip.

This work quantifies the effect of the tip mass on the Sader calibration method, using an Euler-Bernoulli beam with a rigid tip to model the AFM probe. The error in the spring constant estimated by the conventional

Sader method is shown to be on the order of the ratio between the tip mass and the beam's mass. The analysis also reveals a procedure by which one can estimate the mass of the tip from the first few natural frequencies of the probe, allowing one to check whether the calibration might be in error due to the neglected tip and to correct those errors. This procedure is applied to six AFM cantilevers from various manufacturers and the results suggest the tip mass can be reliably estimated for some of the probes. For others the procedure does not seem to be successful. One of those probes is examined in detail and found to taper considerably from root to tip. The mode shapes of the probe in question are measured experimentally and compared with the analytical mode shapes for a uniform beam with a tip mass, suggesting that the taper of this particular probe has a significant effect on its dynamics.

This work focuses on calibration for static rather than dynamic AFM, but these results have important implications for some dynamic imaging methods such as ultrasonic AFM [26], higher harmonic imaging [27] (also see [28, 29]), and multi-frequency imaging [30, 31]; those methods all involve the higher modes of the probe, which are found here to be quite sensitive to the presence of the tip.

2. Effect of Tip Mass on Calibration Method of Sader

The method of Sader will be extended here to include the mass effect of the probe tip using the Ritz method [25]. The calibration method derived here reduces to Sader's method when the tip mass and inertia are zero. The method of Sader is derived by solving a coupled fluid-structure interaction problem to predict the natural frequency and Q-factor of a cantilever in a viscous fluid. The model is then inverted to solve for the beam's static stiffness k_s and area density $\rho_c h$ from the experimentally measured natural frequency and Q-factor.

Sader modeled the forces that a viscous fluid exerts on a vibrating cantilever beam in [32], solving the equation of motion for the fluid surrounding a beam and transformed it into the frequency domain, yielding the force, $F_{hydro}(x,\omega)$, that the fluid applies to a differential cross section of the cantilever beam as a function of the beam's displacement $W(x,\omega)$.

$$F_{hydro}\left(x,\omega\right)=\frac{\pi}{4}\rho_f\omega^2 b^2\Gamma\left(\omega\right)W\left(x,\omega\right) \tag{1}$$

The force that the fluid exerts on the beam depends on the fluid density ρ_f, the frequency of vibration ω, the beam's width b, and the hydrodynamic function $\Gamma(\omega)$. The hydrodynamic function is a complex function of

frequency whose solution, given in [9, 32][2], was used in all of the following. The imaginary part of the hydrodynamic force, due to the imaginary part of $\Gamma(\omega)$, acts as a dissipative term, and is responsible for vibration damping. The real part acts as a mass term. The solution of the fluid equations assumes a long cantilever beam with rectangular cross section, whose width greatly exceeds its thickness.

We shall employ the Ritz method to account for the probe tip by representing the out of plane motion of the cantilever, $w(x,t)$, as a sum of spatial shape functions multiplied by time varying amplitude functions. The displacement then becomes the following in the time and frequency domains respectively.

$$w(x,t) = \sum_{n=1}^{N} \psi_n(x)\, y_n(t) \qquad \Leftrightarrow \qquad W(x,\omega) = \sum_{n=1}^{N} \psi_n(x)\, Y_n(\omega) \tag{2}$$

These expressions are inserted into the kinetic energy, potential energy, power dissipation and power input relationships for the beam, which are given in [25], to find the mass and stiffness matrices governing the amplitudes $y_n(t)$ of the basis functions $\psi_n(x)$ of the Ritz series. As Sader did, we shall limit the description to a single term series N=1 and employ a mode function for a cantilever beam as the basis function. This gives a precise single degree-of-freedom description of the motion of the beam due to that mode.

After including the hydrodynamic force and the mass and inertia of the tip, the frequency domain equation of motion becomes

$$\begin{aligned}\left[\left(\rho_c hbL + \frac{\pi}{4}\rho_f b^2 L \Gamma_r(\omega)\right) m_{nn} + m_{tip}\left(\psi_n(1)\right)^2 + \frac{I_{tip}}{L^2}\left(\psi_n'(1)\right)^2\right]\left(-\omega^2 Y\right) + \\ \left[\frac{\pi}{4}\rho_f \omega b^2 L \Gamma_i(\omega) m_{nn}\right] i\omega Y + \left[\frac{k_s}{3} k_{nn}\right] Y = 0\end{aligned} \tag{3},$$

where ρ_c is the mass density of the cantilever, h and L are the height and length of the cantilever respectively, m_{tip} is the mass of the tip, I_{tip} its mass moment of inertia, and ()′ denotes differentiation with respect to x. The static spring constant, k_s, of the cantilever is given by, k_s = E*bh^3/(4L^3) for a uniform, straight cantilever, where E is the modulus of elasticity of the cantilever. The constants m_{nn} and k_{nn} are given by

[2] Note that the Bessel functions in the solution for the hydrodynamic function in [21] are Bessel functions of the second kind (hence the nomenclature K), not the third kind (Hankel functions) as stated in Sader's paper.

$$m_{nn} = \int_0^1 \left(\psi_n(x)\right)^2 dx$$
$$k_{nn} = \int_0^1 \left(\frac{d^2}{dx^2}\psi_n(x)\right)^2 dx \quad (4).$$

Factoring the total effective mass of the beam, $m_{b,eff} = \rho_c hbL\left(1 + m_{fr}\Gamma_r(\omega)\right)$, out of the mass term and the beam mass out of the damping term, the equation of motion can be rewritten as,

$$\rho_c hbL\left(1 + m_{fr}\Gamma_r(\omega)\right)\left[m_{nn} + m_r\left(\psi_n(1)\right)^2 + m_r\left(\frac{r_g}{L}\right)^2\left(\psi_n'(1)\right)^2\right]\left(-\omega^2 Y\right) +$$
$$\rho_c hbL\left[m_{fr}\Gamma_i(\omega)m_{nn}\right]i\omega Y + \left[\frac{k_s}{3}k_{nn}\right]Y = 0 \quad (5),$$

where m_r is the ratio of the tip mass to the total effective beam mass, $m_{b,eff}$, given by

$$m_r = \frac{m_{tip}}{\rho_c hbL\left(1 + m_{fr}\Gamma_r(\omega)\right)} \quad (6),$$

r_g is the radius of gyration of the probe tip about its center of mass, and m_{fr} is the ratio of the effective mass of the fluid to the beam mass,

$$m_{fr} = \frac{\pi\rho_f b}{4\rho_c h} \quad (7).$$

The effective mass of the fluid is only important if the fluid density times the width of the cantilever is not small relative to the cantilever density times its thickness. In air m_{fr} is generally quite small but in water it is important. Also note that material damping has not been included, so this model is only appropriate if Q is large so that the contribution of material damping can be neglected.

This Ritz model gives an accurate description of the single-mode behavior of the cantilever if the basis function used to construct it is a mode function for the system. The effect of the tip has been included in eqs. (3) and (4), so a mode function for a cantilever with a tip, $\psi_n(x)_{tip}$, should be used in eqs. (4) to find the values of m_{nn} and k_{nn} and to compute the two terms in eq. (5) that account for the tip's mass and inertia. One possible model for $\psi_n(x)_{tip}$ is given in Section 2.1 and is applied to calibrate some commercial probes in Section 3. With m_{nn} and k_{nn} known, one can divide eq. (5) through by the mass factor and then the terms multiplying $i\omega Y$ and Y are ω_n/Q and $\omega_n{}^2$ respectively. This gives two equations for the Q-factor and natural frequency for the system.

Sader noted that if the Q-factor and natural frequency are measured experimentally, then one can invert the procedure to solve for the area density $\rho_c h$ and the cantilever stiffness k_s. Doing so, we obtain the following.

$$\rho_c h = \frac{\pi}{4}\rho_f b\left(Q\Gamma_i(\omega) - \Gamma_r(\omega)\right) - \rho_c h m_r \frac{\left(\psi_n(1)\right)^2}{m_{nn}} - \rho_c h m_r \left(\frac{r_g}{L}\right)^2 \frac{\left(\psi_n'(1)\right)^2}{m_{nn}} \tag{8}$$

$$k_s = \frac{3\pi\rho_f b^2 L m_{nn}\Gamma_i(\omega)}{4k_{nn}} Q\omega_n{}^2 \tag{9},$$

Equations (8) and (9) reduce exactly to the expressions given by Sader et al. [9] if m_r = 0 and r_g = 0 (e.g. if the tip's mass is negligible) and when the first eigenfunction for a cantilever without a tip is used so that $\psi_n(x)$ = $\psi_1(x)_{free}$ in (4), (8) and (9).

Using the conventional method of Sader, one typically measures the Q-factor experimentally and assumes values for the other parameters in the first term on the right in eq. (8) and uses that equation with m_r = r_g = 0 to find $\rho_c h$. Equation (8) reveals that such an approach will overestimate the true area density if either the tip mass ratio or the tip's radius of gyration are significant. On the other hand, eq. (9) for the static stiffness is identical to that presented by Sader. The tip mass and inertia cancel in the derivation of eq. (9) and so they do not appear directly. However, the terms m_{nn} and k_{nn} do depend on the eigenfunction chosen, and so eq. (9) is only precise if an eigenfunction for a cantilever with a tip, $\psi_n(x)_{tip}$, is used to compute m_{nn} and k_{nn}; this is not typically done when employing Sader's method.

If the tip mass could be adequately estimated, for example from SEM images of the tip, then one could use beam theory to compute $\psi_n(x)_{tip}$ and use eqs. (8) and (9) to correctly calibrate a probe even when a significant tip is present. Unfortunately, SEM metrology is difficult and time consuming, so such an approach is usually not practical. The remainder of this work uses a simple model of a cantilever with a probe tip to show how the tip mass ratio can be estimated from measurements of some of the higher natural frequencies of the probe and also estimates the error that one incurs if the tip is not accounted for.

If the conventional Sader method is used, the error in the estimated spring constant depends on the difference between the actual eigenfunction, $\psi_n(x)_{tip}$, and that of the tip-less Euler-Bernoulli model that was used by Sader. If the tip-less eigenfunctions are used then the values m_{nn} and k_{nn} in eq. (9) will be in error. Denoting

the values that neglect the tip as m_{nn} and k_{nn} and the values that account for the tip as $\hat{m}_{nn}$ and $\hat{k}_{nn}$, the error in the static stiffness is

$$err(k_s)_n = \frac{k_s - k_{s,true}}{k_s} = 1 - \frac{\hat{m}_{nn}}{\hat{k}_{nn}} \frac{k_{nn}}{m_{nn}} \tag{10}.$$

A scale factor on the eigenfunctions would cancel in this relationship, so the error depends only on how much the mode shape of the probe changes due to the tip. Similarly, the error in the area density identified by the conventional Sader method is

$$err(\rho_c h)_n = m_r \frac{\left(\psi_n(1)\right)^2}{m_{nn}} + m_r \left(\frac{r_g}{L}\right)^2 \frac{\left(\psi_n'(1)\right)^2}{m_{nn}} \tag{11}.$$

All of the preceding has presumed that the n-th mode of a cantilever was used in the calibration. Sader derived his calibration approach assuming that the first mode would be used, but one could use any mode as illustrated by the preceding discussion. It may be preferable to use a higher mode when the fundamental mode cannot be accurately identified due to narrow band noise or heavy damping, or to verify the result obtained by calibrating based on the fundamental mode. One should also note that the error analysis presented in this section could be extended to probes of other geometries by replacing the Ritz vector used here with an appropriate mode function. Dynamic models for triangular, picketed and membrane (FIRAT) probes are described in [33] and the works referenced there, and these could be coupled with a suitably modified fluid-structure model, such as that in [34], to treat those probes. As was the case with the beam model considered here, the error incurred due to the neglected tip would depend on how much the tip mass changes the shape of the dynamic mode used in the calibration.

2.1. Analytical Model for a Rectangular Cantilever Including the Tip's Mass Effect

To evaluate the error in the stiffness (eq. (10)), we require an estimate for the mode functions of a cantilever with a tip mass. The modes of an Euler-Bernoulli cantilever beam with a rigid tip have been presented in [35, 36], and are relatively straightforward to derive using the procedure outlined in the text by Ginsberg [25]. More advanced models are also available, such as the Timoshenko beam model presented recently by Mahdavi et al. [37]. This work uses an Euler-Bernoulli model to facilitate comparison with the Sader method. The mode

shape of an Euler-Bernoulli cantilever with constant mass density, ρ_c, modulus of elasticity, E, and area moment of inertia, I, and with a rigid tip at the extreme of its free end is

$$\psi_n(x) = \sin(\alpha_n x) - \sinh(\alpha_n x) + R_n\left(\cos(\alpha_n x) - \cosh(\alpha_n x)\right) \quad (12),$$

where

$$R_n = -\frac{\sin(\alpha_n) + \sinh(\alpha_n)}{\cos(\alpha_n) + \cosh(\alpha_n)} \quad (13),$$

and the parameter α_n is found by satisfying the boundary conditions. Once α_n is known, the nth natural frequency ω_n is found from,

$$\omega_n^2 = \frac{EI\alpha_n^4}{m_{b,eff}L^3} \quad (14).$$

For a beam without a tip, as used in the conventional Sader method, the constants are $(\alpha_1)_{free}$ = 1.8751 and $(R_1)_{free}$ = -1.3622, and the terms m_{11} and k_{11} are 1.8556 and 22.94 respectively. A rigid tip modifies the boundary condition at the free end of the cantilever. Using the approach outlined in [25] or [36] and assuming that the center of mass of the tip is located a negligible distance from the end of the cantilever as measured along the axis of the cantilever, the boundary conditions are the following in non-dimensional form.

$$\frac{d^2\psi_n(x)}{dx^2} + \alpha_n^4 m_r\left(\frac{r_g}{L}\right)^2\frac{d\psi_n(x)}{dx} = 0 \quad (15)$$

$$\frac{d^3\psi_n(x)}{dx^3} + \alpha_n^4 m_r\psi_n(x) = 0 \quad (16)$$

One can use these equations, in conjunction with eqs. (12) and (13) to obtain the constants $(\alpha_n)_{tip}$ and $(R_n)_{tip}$ for a certain m_r and r_g, as described in [25, 36]. For parameters typical of AFM cantilever probes, the radius of gyration $r_g << L$, so it can be neglected, although even a small radius of gyration may be important for the higher order modes. The tip mass model was evaluated for various values of the tip mass ratio with r_g = 0, and the constants $(\alpha_n)_{tip}$ that were found are given in the Appendix. Note that these constants depend only on the mass ratio, m_r, so they can be used for a variety of cantilevers having any width, thickness, modulus, length and density, so long as the standard assumptions of Euler-Bernoulli beam theory and of the fluid structure interaction theory [9, 32] are not violated.

To facilitate comparisons with the experimental measurements in the following sections, it is convenient to compute the ratios of the natural frequencies to the first using eq. (14), in order to eliminate the dependence on $EI/m_{b,eff}L^3$. The frequency ratios for the first six modes are given in Table 1 for various mass ratios. The ratios in the table show that the natural frequencies of a probe become more widely spaced relative to the first as the tip mass increases. The frequency spacing increases monotonically with tip mass, so the frequency ratios can be used to identify the mass ratio by solving the equations above, or by simply interpolating using this table. This is pursued in Section 3.1 for a number of commercial probes.

Frequency Ratio	**Mass Ratio** m_r						
	0	0.02	0.04	0.1	0.2	0.4	0.8
ω_2/ω_1	6.27	6.28	6.32	6.52	6.97	7.92	9.66
ω_3/ω_1	17.55	17.63	17.82	18.71	20.50	24.01	30.05
ω_4/ω_1	34.39	34.60	35.11	37.30	41.41	49.10	61.99
ω_5/ω_1	56.84	57.30	58.32	62.45	69.82	83.28	105.53
ω_6/ω_1	84.91	85.73	87.47	94.19	105.76	126.54	160.66

Table 1: Ratios of natural frequencies to the first for Euler-Bernoulli beam with various tip-beam mass ratios m_r with $r_g = 0$.

2.2. Calibration Errors Based on Euler-Bernoulli Model

Assuming that the analytical Euler-Bernoulli model discussed in the previous section accurately represents a real probe with a tip, we can compute the error in the stiffness identified by the Sader method for a range of mass ratios using eq. (10). Table 2 shows the ratio of the true stiffness to that estimated using the conventional method of Sader (tipless beam model) for various tip mass ratios. The error is less than 2% if the first mode of the cantilever is employed in the calibration, even for large tip mass to beam mass ratios. On the other hand, the error can be considerable if the second or higher modes of vibration are used to perform the calibration, especially for mass ratios greater than m_r = 0.1.

% Error in k_s for each mode	**Mass Ratio** m_r					
	0.02	0.04	0.1	0.2	0.4	0.8
$err(k_s)_1$	0.0%	0.1%	0.3%	0.6%	1.1%	1.7%
$err(k_s)_2$	-0.5%	-1.7%	-8.0%	-20.2%	-39.6%	-61.1%
$err(k_s)_3$	-0.8%	-2.8%	-10.1%	-20.1%	-31.0%	-39.8%
$err(k_s)_4$	-1.2%	-3.5%	-10.5%	-17.7%	-24.3%	-28.8%
$err(k_s)_5$	-1.4%	-3.9%	-10.1%	-15.5%	-19.7%	-22.5%
$err(k_s)_6$	-1.6%	-4.1%	-9.5%	-13.6%	-16.6%	-18.4%

Table 2: Error in the spring constant when using the conventional method of Sader, estimated using eq. (10) for various m_r and with r_g = 0.

The Sader method also allows one to estimate the area density, $\rho_c h$, of an AFM probe. Table 3 shows the percentage error in the estimated area density for various tip mass ratios, computed using eq. (8). As expected, the Sader method always overestimates the density, attributing the mass of the tip to the cantilever beam. For the first mode, the effective mass of the beam is about one fourth its total mass, so the fact that the error values are about four times higher than the mass ratios seems reasonable. On the other hand, the error decreases for the higher modes of the beam, due to the interplay between the mass effect and the change that it induces in the mode shapes.

% Error in $\rho_c h$ for each mode	**Mass Ratio m_r**					
	0.02	0.04	0.1	0.2	0.4	0.8
$err(\rho_c h)_1$	8.0%	16.1%	40.7%	82.2%	166.1%	334.9%
$err(\rho_c h)_2$	7.0%	12.1%	20.0%	21.8%	17.9%	11.7%
$err(\rho_c h)_3$	6.2%	9.6%	12.1%	10.5%	7.2%	4.2%
$err(\rho_c h)_4$	5.5%	7.6%	8.0%	6.1%	3.8%	2.1%
$err(\rho_c h)_5$	4.8%	6.2%	5.6%	3.9%	2.3%	1.3%
$err(\rho_c h)_6$	4.3%	5.1%	4.2%	2.7%	1.6%	0.9%

Table 3: Percentage error in the area density estimated using the conventional method of Sader, computed using eq. (11) for various tip mass ratios, for various m_r and with r_g = 0.

3. Experimental Verification

The methods presented here were applied to a number of commercially available AFM cantilever probes. Table 4 list the manufacturer specifications of the cantilevers used, all of which are contact mode cantilevers with relatively low spring constants, as might be used for high sensitivity force measurements or contact mode imaging on delicate surfaces. CSC38-B and -C are Mikromasch™ "38th series" contact mode, silicon nitride cantilevers, VCO denotes a Veeco™ MP-32220-10 Phosphorus (n) doped Silicon cantilever, HYDRA denotes a HYDRA6R-200N silicon nitride, contact mode probe with a single-crystal silicon tip, available from NanoScience Instruments™, BSI is a PPP-BSI-SPL n-Silicon cantilever from Nanosensors™, and NW denotes a PNP-DB silicon nitride cantilever from NanoWorld™. Not all of the desired specifications were available from the manufacturers; the values denoted with * were estimated based on the manufacturer's images and other specifications. The last column presents our estimate of the tip mass ratio for each cantilever. This was computed from the manufacturer's specifications regarding the tip height, shape, angle and based on the SEM

images available in the product literature. Those mass ratios are not expected to be very accurate, but are simply meant to represent the best estimate of the mass ratio that one might obtain without imaging or otherwise measuring the size of the tip.

Cantilever	Cantilever Length L (μm)	Cantilever Width b (μm)	Cantilever Thickness h (μm)	Resonant Frequency (kHz)	Spring Constant (N/m)	Tip Height (μm)	Tip Mass Ratio m_r (estimated)
BSI	225 ± 10	28 ± 7.5	1 ± 0.5	12 – 45	0.01 – 0.5	10 - 15	8 - 12%*
CSC38-B	350 ± 5	35 ± 3	0.7 - 1.3	7.0 - 14	0.01 - 0.08	20 – 25	8.3 - 9.7%*
CSC38-C	250 ± 5	35 ± 3	0.7 - 1.3	14 - 28	0.02 - 0.20	20 - 25	12 - 14%*
HYDRA	200	35	0.6	17	0.035	5	9.4 - 16%*
NW	200	40	0.6	17	0.06	3.5	0.35%*
VCO	515 - 535	25 - 35	1.5 - 2.5	9 - 13	0.1	15-20*	1.5 - 3.6%*

Table 4: Manufacturer specifications for AFM probes used in this study.

The thermal vibration of each of the probes was measured with the probes mounted in a Digital Instruments Nanoscope™ IV AFM, using a Tektronix DPO4032 oscilloscope to record between 1 and 10 million samples of the thermal vibration at a sample rate of either 1.0 or 2.5 MHz. The thermal spectra were then estimated offline using between 50 and 87.5% overlap and with an adequate frequency resolution to assure that there were at least 3-4 frequency lines in the half power bandwidth for each mode. Figure 2 shows the thermal spectrum measured for the BSI cantilever. Four modes are present in the Up-Down (bending) signal, two modes in the Left-Right (torsion). Numerous spurious peaks exist, but most are sharp and quite easy to distinguish from the bending and torsional modes of the probe. These thermal spectra were typical of all of those obtained. Thermal spectra were used in lieu of the biomorph driven spectra used to tune tapping mode cantilevers, because the driven spectra tended to exhibit many additional resonances that were difficult to distinguish from the cantilever modes and because there were some anomalies with the Nanoscope IV controller that cast doubt on the accuracy of those spectra.

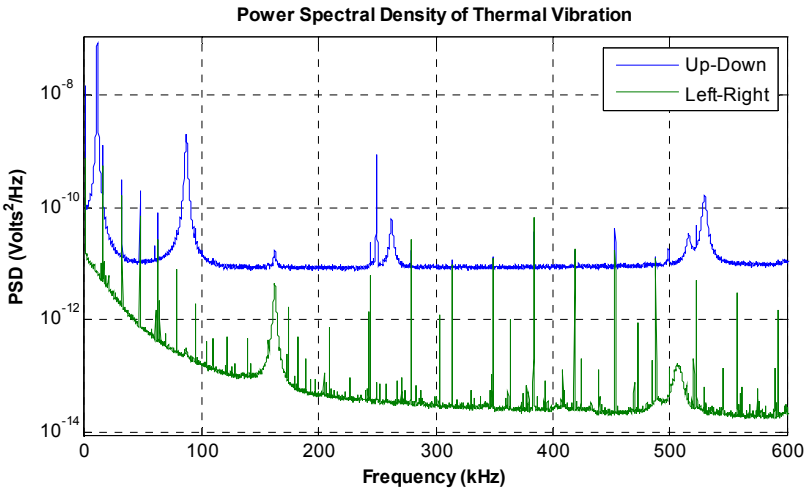

Figure 2: Thermal spectrum of the HYDRA cantilever

Table 5 shows the natural frequencies and Q-values identified from the thermal spectra for each of the cantilevers. A different approach was used to test the CSC38-B cantilever; it was tested in near vacuum using a Polytec MSV-400 Laser Doppler Vibrometer focused through a Mitutoyo optical microscope, using the setup described in [38]. Its Q-values were very high and are not necessarily dominated by the effect of the air, so they are not reported.

Probe	Natural Frequencies (kHz)				Q-values			
	f_1	f_2	f_3	f_4	Q_1	Q_2	Q_3	Q_4
BSI	19.0	126.2	362.3	-	29.1	84.6	143.1	-
CSC38-B	9.1	70.8	213.8	439.8	*test performed at 7mTorr*			
CSC38-C	10.9	95.2	300.7	-	33.9	78.5	136.6	-
HYDRA	10.9	86.9	262.5	-	28.0	52.0	70.1	-
NW	13.2	82.8	231.8	-	25.4	80.5	156.1	-
VCO	10.2	64.6	184.9	367.2	31.8	107.9	172.3	362.9

Table 5: Natural Frequencies and Q-values identified from the cantilevers used in this work.

3.1. Estimating the Probes' Tip Mass Ratio

As mentioned previously, the ratios of the natural frequencies can be used to determine whether the tip is significantly affecting a probe's dynamics. Table 6 shows the ratios of the natural frequencies to the fundamental for of each of the six probes. Comparing these ratios with those presented in Table 1, it is clear that the frequency spacing for many of these probes does not agree with an Euler-Bernoulli model for a tip-less probe. Each of these experimentally measured frequency ratios was used to estimate the mass ratio by linearly interpolating each ratio on Table 1 and noting the corresponding value of m_r. The mass ratios found are shown in

the table, with $(m_r)_n$ corresponding to the mass ratio found by interpolating the ratio of the nth frequency to the first. (Note that these are reported in percent.)

Probe	Ratios of Natural Frequencies			Interpolated Mass Ratios m_r (%)		
	f_2/f_1	f_3/f_1	f_4/f_1	$(m_r)_2$	$(m_r)_3$	$(m_r)_4$
BSI	6.64	19.06	-	12.6%	12.0%	-
CSC38-B	7.81	23.57	48.49	37.6%	37.5%	38.4%
CSC38-C	8.76	27.65	-	59.2%	64.1%	-
HYDRA	8.00	24.17	-	41.7%	41.0%	-
NW	6.27	17.56	-	0.27%	0.33%	-
VCO	6.32	18.08	35.91	3.7%	5.8%	6.2%

Table 6: Ratios of the Natural Frequencies in Table 5 and tip mass ratios estimated from each natural frequency ratio by interpolating on Table 1.

There is fairly good consistency between the interpolated mass ratios for all of the probes, and most of the interpolated mass ratios are significantly greater than zero. The interpolated NW and VCO mass ratios are relatively small, so, based on the results in Table 2, one would expect the conventional Sader method to work quite well to calibrate those probes no matter which mode was used to perform the calibration.

The interpolated mass ratios for the BSI, NW and VCO probes agree quite well with those estimated from the manufacturer specifications in Table 4. On the other hand, the ratios for the HYDRA probe and for both CSC probes are as much as four times larger than expected based on the specifications.

3.2. Detailed Measurements for CSC38-B

Additional tests were performed on the CSC38-B cantilever to search for the source of the large discrepancy between the interpolated mass ratio and the manufacturer specifications. A detailed SEM image of the tip of a CSC38-B cantilever was obtained, similar to that which was shown in Figure 1. For logistical reasons, this was not the same cantilever as that from which the measurements in Table 6 were taken, but it was from the same lot. This SEM image was used to estimate the volume of the tip by approximating it as a cone with base radius and height of 7.75 and 20.0 microns respectively, from which we obtained a volume of 1260 μm^3. Using the nominal dimensions of the cantilever, the beam volume was estimated to be 8750 μm^3, so if the density of the probe tip and beam are equivalent then the mass ratio is 0.103. The radius of gyration was estimated to be r_g = 4.9 μm, which is much less than the length of the beam. Of course, there is considerable uncertainty associated with this calculation of the mass ratio, first because the tip is not a perfect cone and second because the SEM's scale bar is only accurate to within 5-10%; it was noted that the SEM gives the cantilever's total length as 323

microns, where the manufacturer's specification is 350 $\pm$ 5 microns, 8% higher. Finally, one would expect that the density of the silicon nitride from which the tip is made could be significantly different from the average density of the cantilever.

The mode shapes of two CSC38-B cantilevers were obtained using the laser vibrometer system mentioned previously. One CSC38-B probe was tested in air at a pressure of about 86 kPa, while the other was tested in near vacuum (~7mTorr) to minimize dissipation and improve the vibration signals. The first four operating deflection shapes and their peak frequencies were extracted from the probe tested at 7mTorr, while only the first two were obtained from the probe tested at ambient pressure. Considering the high quality factor of the modes in both cases, the operating deflection shapes (ODSs) give a very good approximation of the mode shapes of the probes. The measured operating shapes are shown in Figures 3 through 6. The mode shapes obtained from the analytical model are also shown for mass ratios of m_r = 0, 0.1, 0.2, 0.4 and 1.6. The operating shapes obtained experimentally cannot be easily mass normalized, so all of the shapes shown in Figures 3 through 6 were simply scaled to have a unit-norm if interpolated onto a common set of x-positions. Circles are shown for the operating shapes that were measured in vacuum, crosses for those measured in ambient conditions. The operating shapes were measured at both edges of the probe, as viewed when looking down from the top, and a marker is plotted for each edge and at each x location. The measurements usually overlay one another at each x location, indicating that torsion of the beam is negligible.

The analytical mode shapes in Figure 3 all lay essentially on top of one another, revealing that the first mode shape is not very sensitive to the presence of the tip, even for very large mass ratios. The tip does change the scale of the mass normalized mode shape (not shown), but the shape, which is the important factor in Sader calibration, remains essentially unchanged. The first operating shape measured in both air and vacuum agrees very well with any of the analytical shapes.

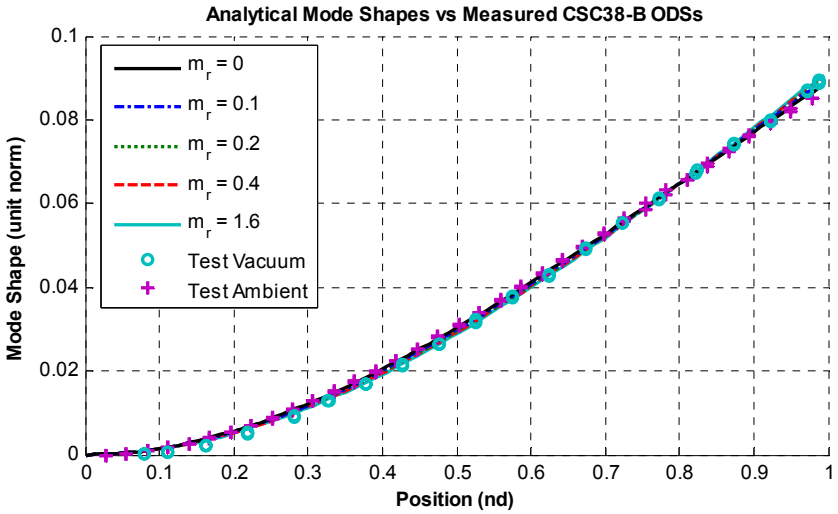

Figure 3: Experimentally measured first mode shape for two cantilever AFM probes in vacuum (o) and in air (+) and analytical mode shapes for various tip mass ratios m_r (lines).

Figure 4 compares the experimental and analytical shapes of the second mode. The tip has a much larger effect on the second mode of the AFM probe; the analytical mode shape changes noticeably for m_r = 0.1, and its magnitude near the right end of the beam decreases substantially as the mass ratio increases further. The experimental measurements of the 2nd operating shape agree with one another fairly well, and envelope the model for m_r = 0.1.

Figures 5 and 6 illustrate that the 3rd and 4th modes are even more sensitive to the presence of the tip mass, especially near the end of the beam. The node lines of the beam move to the right as the mass ratio increases, although the most significant effect is the reduction in the amplitude of the beam's motion near the end. For example, for m_r = 0.1 the beam's motion at the end is half of that at the mid span in the 4th mode of vibration, while the two are almost equal if the tip mass is not present. The experimentally measured 3rd and 4th operating shapes show about the same amplitude of motion near the end of the beam as the analytical ones for m_r = 0.1. However, there are substantial differences in the shapes over the rest of the beam. This is most notable for the 4th mode, where the depths of the two valleys in the experimental shape are quite different from those in the analytical model.

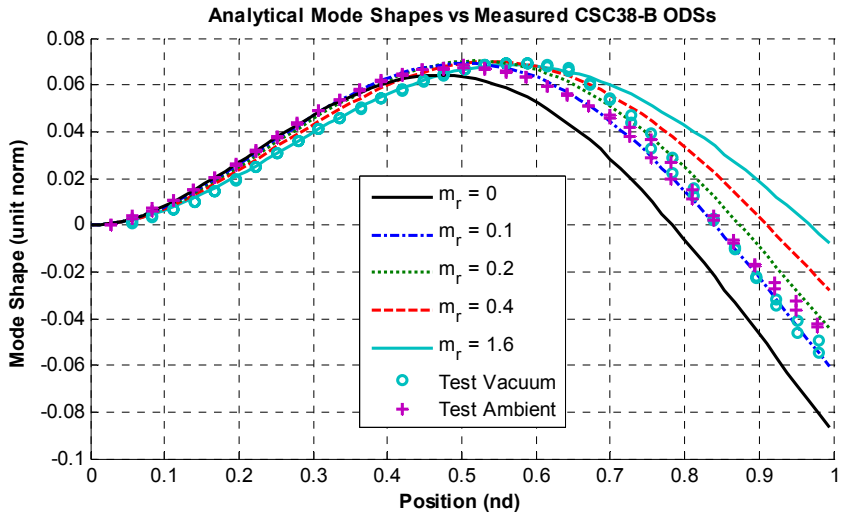

Figure 4: Experimentally measured second mode shape for two cantilever AFM probes in vacuum (o) and in air (+) and analytical mode shapes for various tip mass ratios m_r (lines).

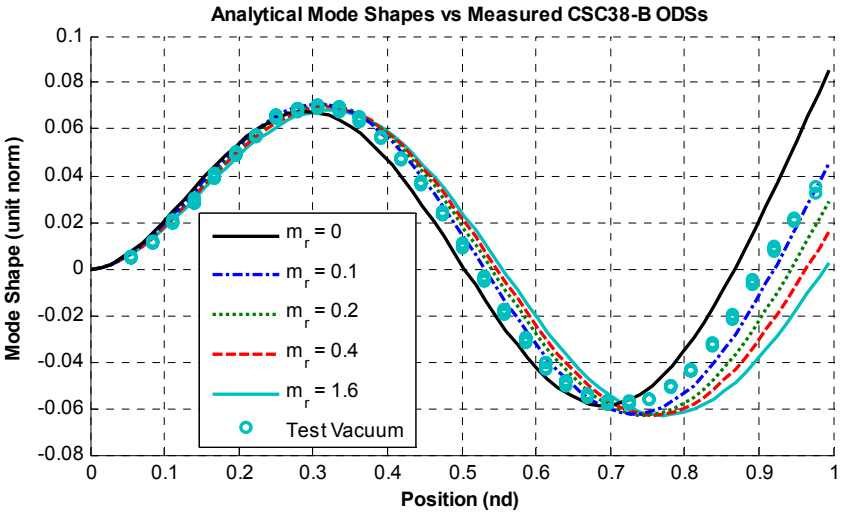

Figure 5: Experimentally measured third mode shape for a CSC38-B AFM probe in vacuum (o) and analytical mode shapes for various tip mass ratios m_r (lines).

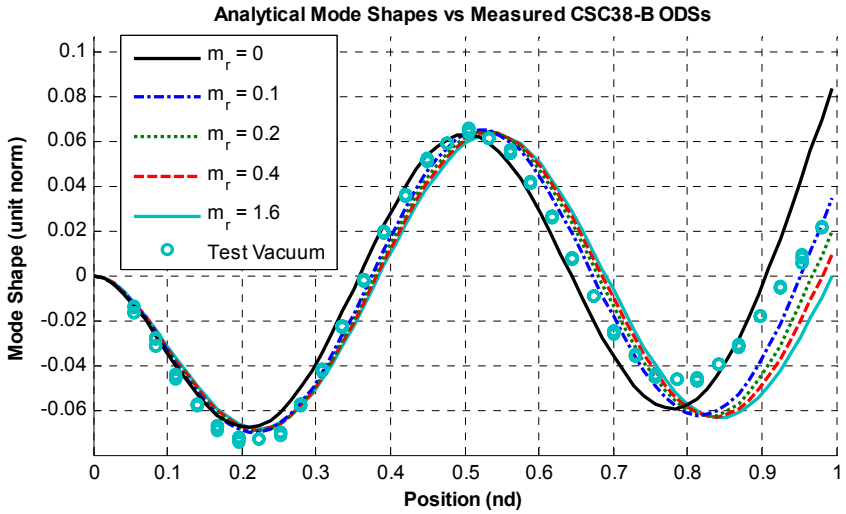

Figure 6: Experimentally measured fourth mode shape for a CSC38-B AFM probe in vacuum (o) and analytical mode shapes for various tip mass ratios m_r (lines).

Discussion

The experimental measurements show that the tip does have a significant effect on the modes of the CSC38-B probe. The analytical model of the probe including the tip's mass-loading effect, developed in Section 2.1, agrees with the measurements in some aspects, but not in others. The model suggests that the first mode shape of the cantilever is quite insensitive to the presence of the tip, and experimental measurements do not contradict this. The frequency and modal scale factor for the first mode do change due to the inclusion of the tip mass, but the analysis in Section 2.2 shows that this does not affect the Sader calibration method. The work by Melcher, Hu & Raman also reported that the inclusion of a sizable mass on the end of a cantilever beam did not significantly change either the shape of the first mode nor its effective stiffness [33]. The second mode shape is affected by the tip, and the second measured mode shape agrees well with that predicted by theory for m_r = 0.1, which is near the SEM estimated mass ratio of 0.103. On the other hand, the measured 3rd and 4th mode shapes deviate from the model over much of the probe and the frequency ratios of the cantilever are different than those predicted analytically for the experimentally estimated mass ratio.

Additional SEM images were acquired from a CSC38-B cantilever to search for the source of the discrepancies between the experimental measurements and the model and are shown in Figure 7; these show the same cantilever pictured in Figure 1. These images show that the probe is significantly thinner near the root than its specification, and more than three times thicker near the tip. Initial efforts to model this effect reveal that the frequency ratios of a cantilever are very sensitive to thickness non-uniformity; this probably explains the discrepancies between the interpolated mass ratios in Table 6 and the mass ratio estimated from the SEM

images. This is of concern because a beam with the thickness profile shown here would have a much different static stiffness than a uniform beam because the beam is much thinner in a critical location. These results suggest that one should be wary of the results of a dynamic calibration if a particular probe's modes are not spaced as one would expect for a reasonable mass ratio. The mass ratios estimated for the HYDRA probe in Table 6 are also much larger than expected, so that probe should also be evaluated carefully, although this will not be pursued here. It is interesting to note that both the CSC and HYDRA probes have silicon nitride cantilevers, which are potentially more susceptible to non-uniformity than the silicon cantilevers due to the manufacturing process employed.

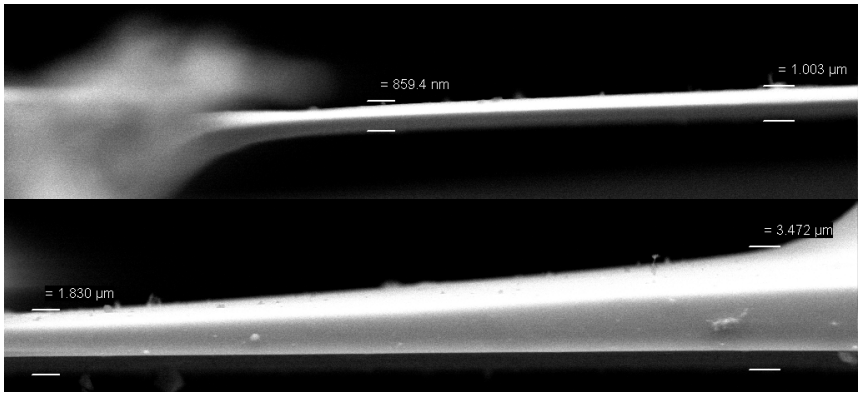

*Figure 7: SEM Images of portions of the CSC38-B AFM cantilever shown in Figure 1**Error! Reference source not found.**, revealing that the thickness of the cantilever is not uniform along its length.*

3.3. Calibration Results

The Sader method was used to calibrate each of the six probes using each mode independently in eq. (9), resulting in the spring constants shown in Table 7. The average of the mass ratios identified in Table 6 was used in the calibration and the radius of gyration was set to zero. The CSC and HYDRA probes were not included because their frequency ratios suggest that they are not well modeled by the Euler-Bernoulli model upon which calibration is based. The results in Table 7 show a fair amount of scatter in the spring constants estimated from each mode for the same probe. The 4^{th} mode of the VCO probe was almost buried in the background noise, so one would expect that the Q-value for that mode might be somewhat unreliable, but the other Q-values all reconstructed the measured thermal spectra quite well. The estimated spring constants for the first three modes are all within $\pm$ 10% of their mean values, and are reasonably close to the manufacturer's specifications.

Probe	Estimated Spring Constants (N/m)				
	K_1	K_2	K_3	K_4	$mean(K_{1\text{-}3})$
BSI	0.0513	0.0590	0.0603	-	0.0569
NW	0.0314	0.0336	0.0377	-	0.0343
VCO	0.0602	0.0664	0.0622	0.0944	0.0629

Table 7: Spring constants estimated using the modified method of Sader for each identified mode. These values were computed using eq. (9) with the mass-ratio set to the average of the values in Table 6 and the radius of gyration of the tip equal to zero.

4. Conclusions

This work has explored the effect of the probe tip on the accuracy of the Sader [8] Atomic Force Microscope probe calibration method. A simple Euler-Bernoulli model was derived for a cantilever with a rigid mass on its tip and was used to estimate the error incurred due neglecting the tip's inertial effect. The model revealed that the Sader method may accurately estimate the cantilever's stiffness even if the tip mass is quite large, but only if the first mode is used in the calibration. For some probes it may be difficult to measure the Q-factor of the first mode due to instrument noise or other anomalies, and in any event it may be helpful to calibrate a probe using a number of different modes so one can check for errors. This work has also presented a modification to the method of Sader that allows one to calibrate a probe based on the second or higher modes and has shown that the tip should be considered if the tip's mass is significant relative to the beam's mass.

The analytical model also revealed that the ratios between the natural frequencies of a cantilever are sensitive to the tip mass, so this can be used to estimate the tip mass ratio and to correct the calibration. This was verified experimentally by measuring the natural frequencies of a number of commercially available cantilevers and comparing them with the model. Three of the probes, the BSI, VCO and NW probes, all had frequency ratios that agreed well with the model for tip mass ratios near those estimated from the manufacturers specifications. Three other probes, the HYDRA and CSC38-B and CSC38-C both had much larger frequency ratios than predicted by the model for a reasonable mass ratio. One of these probes was imaged using SEM, revealing that the cantilever tapered out from the root to the tip. Preliminary models of this effect suggest that it is responsible for the increased frequency ratios and distortions in the experimentally measured mode shapes. This is an important issue, because a taper such as that which was observed here could result in the probe stiffness being significantly in error. Hence, it seems advisable to compare the frequency ratios of a probe with those of the analytical model whenever dynamic calibration methods are employed, because they can reveal

discrepancies between the dynamics of the actual probe and the model upon which the calibration method is based.

5. Acknowledgements

Part of this work was conducted at Sandia National Laboratories. Sandia is a multi-program laboratory operated under Sandia Corporation, a Lockheed Martin Company, for the United States Department of Energy under Contract DE-AC04-94-AL85000. The authors also wish to acknowledge Hendrik Frentrup for his efforts acquiring and processing the thermal spectra used here.

6. Appendix

Mode	Mass Ratio m_r						
	0	0.02	0.04	0.1	0.2	0.4	0.8
α_1	1.8751	1.8393	1.8065	1.7227	1.6164	1.4724	1.3041
α_2	4.6941	4.6100	4.5420	4.3995	4.2671	4.1444	4.0531
α_3	7.8548	7.7218	7.6251	7.4511	7.3184	7.2155	7.1490
α_4	10.9955	10.8195	10.7043	10.5218	10.4016	10.3178	10.2675
α_5	14.1372	13.9227	13.7955	13.6142	13.5067	13.4367	13.3963
α_6	17.2788	17.0300	16.8954	16.7196	16.6234	16.5634	16.5298

Table 8: α_n values for Euler-Bernoulli beam with various tip-beam mass ratios m_r and with $r_g=0$.

References

[1] R. Garcia and R. Perez, "Dynamic atomic force microscopy methods," *Surface Science Reports,* vol. 47, pp. 197-301, 2002.

[2] R. W. Carpick and M. Salmeron, "Scratching the surface: fundamental investigations of tribology with atomic force microscopy," *Chemical Reviews,* vol. 97, p. 1163, 1997.

[3] G. U. Lee, D. A. Kidwell, and R. J. Colton, "Sensing discrete streptavidin-biotin interactions with atomic force microscopy," *Langmuir,* vol. 10, pp. 354-357, 1994.

[4] E. L. Florin, V. T. Moy, and H. E. Gaub, "Adhesion forces between individual ligand-receptor pairs," *Science,* vol. 264, pp. 415-17, 1994.

[5] V. T. Moy, E.-L. Florin, and H. E. Gaub, "Intermolecular forces and energies between ligands and receptors," *Science,* vol. 266, pp. 257-259, 1994.

[6] S. E. Cross, Y.-S. Jin, J. Rao, and J. K. Gimzewski, "Nanomechanical analysis of cells from cancer patients," *Nat Nano,* vol. 2, pp. 780-783, 2007.

[7] S. E. Cross, Y.-S. Jin, J. Tondre, R. Wong, J. Rao, and J. K. Gimzewski, "AFM-based analysis of human metastatic cancer cells," *Nanotechnology,* vol. 19, p. 384003, 2008.

[8] J. E. Sader, I. Larson, P. Mulvaney, and L. R. White, "Method for the calibration of atomic force microscope cantilevers," *Review of Scientific Instruments,* vol. 66, p. 3789, 1995.

[9] J. E. Sader, J. W. M. Chon, and P. Mulvaney, "Calibration of rectangular atomic force microscope cantilevers," *Review of Scientific Instruments,* vol. 70, pp. 3967-9, 1999.

[10] J. L. Hutter and J. Bechhoefer, "Calibration of atomic-force microscope tips," *Review of Scientific Instruments,* vol. 64, pp. 1868-73, 1993.

[11] T. J. Senden and W. A. Ducker, "Experimental determination of spring constants in atomic force microscopy," *Langmuir,* vol. 10, pp. 1003-1004, 1994.
[12] M. Tortonese and M. Kirk, "Characterization of application specific probes for SPMs." vol. 3009 San Jose, CA, USA: SPIE-Int. Soc. Opt. Eng, 1997, pp. 53-60.
[13] J. P. Cleveland, S. Manne, D. Bocek, and P. K. Hansma, "A nondestructive method for determining the spring constant of cantilevers for scanning force microscopy," *Review of Scientific Instruments,* vol. 64, pp. 403-5, 1993.
[14] N. A. Burnham, X. Chen, C. S. Hodges, G. A. Matei, E. J. Thoreson, C. J. Roberts, M. C. Davies, and S. J. B. Tendler, "Comparison of calibration methods for atomic-force microscopy cantilevers," *Nanotechnology,* vol. 14, pp. 1-6, 2003.
[15] H. J. Butt and M. Jaschke, "Calculation of thermal noise in atomic force microscopy," *Nanotechnology,* vol. 6, p. 1, 1995.
[16] T. E. Schaffer, "Calculation of thermal noise in an atomic force microscope with a finite optical spot size," *Nanotechnology,* vol. 16, pp. 664-70, 2005.
[17] S. M. Cook, T. E. Schaffer, K. M. Chynoweth, M. Wigton, R. W. Simmonds, and K. M. Lang, "Practical implementation of dynamic methods for measuring atomic force microscope cantilever spring constants," *Nanotechnology,* vol. 17, pp. 2135-45, 2006.
[18] R. Proksch, T. E. Schaffer, J. P. Cleveland, R. C. Callahan, and M. B. Viani, "Finite optical spot size and position corrections in thermal spring constant calibration," *Nanotechnology,* vol. 15, pp. 1344-1350, 2004.
[19] M. J. Higgins, R. Proksch, J. E. Sader, M. Polcik, S. M. Endoo, J. P. Cleveland, and S. P. Jarvis, "Noninvasive determination of optical lever sensitivity in atomic force microscopy," *Review of Scientific Instruments,* vol. 77, pp. 13701-1, 2006.
[20] B. Ohler, "Cantilever spring constant calibration using laser Doppler vibrometry," *Review of Scientific Instruments,* vol. 78, pp. 63701-1, 2007.
[21] B. Ohler, "Application Note #94: Practical Advice on the Determination of Cantilever Spring Constants," in *Veeco Application Notes*. vol. http://www.veeco.com/library, 2007.
[22] B. Cappella, H. J. Butt, and M. Kappl, "Force measurements with the atomic force microscope: Technique, interpretation and applications," *Surface Science Reports,* vol. 59, pp. 1-152, 2005.
[23] C. P. Green, H. Lioe, J. P. Cleveland, R. Proksch, P. Mulvaney, and J. E. Sader, "Normal and torsional spring constants of atomic force microscope cantilevers," *Review of Scientific Instruments,* vol. 75, pp. 1988-96, 2004.
[24] M. B. Viani, T. E. Schaffer, G. T. Paloczi, L. I. Pietrasanta, B. L. Smith, J. B. Thompson, M. Richter, M. Rief, H. E. Gaub, K. W. Plaxco, A. N. Cleland, H. G. Hansma, and P. K. Hansma, "Fast imaging and fast force spectroscopy of single biopolymers with a new atomic force microscope designed for small cantilevers," *Review of Scientific Instruments,* vol. 70, pp. 4300-4303, 1999.
[25] J. H. Ginsberg, *Mechanical and Structural Vibrations*, First ed. New York: John Wiley and Sons, 2001.
[26] K. Yamanaka, H. Ogisoa, and O. Kolosov, "Ultrasonic force microscopy for nanometer resolution subsurface imaging," *Applied Physics Letters,* vol. 64, 10 January 1994.
[27] S. Crittenden, A. Raman, and R. Reifenberger, "Probing attractive forces at the nanoscale using higher-harmonic dynamic force microscopy," *Physical Review B (Condensed Matter and Materials Physics),* vol. 72, pp. 235422-1, 2005.
[28] O. Sahin, C. F. Quate, O. Solgaard, and A. Atalar, "Resonant harmonic response in tapping-mode atomic force microscopy," *Physical Review B (Condensed Matter and Materials Physics),* vol. 69, pp. 165416-1, 2004.
[29] O. Sahin, G. Yaralioglu, R. Grow, S. F. Zappe, A. Atalar, C. Quate, and O. Solgaard, "High-resolution imaging of elastic properties using harmonic cantilevers," 2-3 ed. vol. A114 Boston, MA, USA: Elsevier, 2004, pp. 183-90.
[30] R. Proksch, "Multifrequency, repulsive-mode amplitude-modulated atomic force microscopy," *Applied Physics Letters,* vol. 89, pp. 113121-1, 2006.
[31] J. R. Lozano and R. Garcia, "Theory of multifrequency atomic force microscopy," *Physical Review Letters,* vol. 100, pp. 076102-1, 2008.
[32] J. E. Sader, "Frequency response of cantilever beams immersed in viscous fluids with applications to the atomic force microscope," *Journal of Applied Physics,* vol. 84, pp. 64-76, 1998.
[33] J. Melcher, S. Hu, and A. Raman, "Equivalent point-mass models of continuous atomic force microscope probes," *Applied Physics Letters,* vol. 91, p. 053101, 2007.

[34] J. E. Sader, J. Pacifico, C. P. Green, and P. Mulvaney, "General scaling law for stiffness measurement of small bodies with applications to the atomic force microscope," *Journal of Applied Physics,* vol. 97, p. 124903, 2005.
[35] C. W. S. To, "Vibration of a Cantilever Beam with a Base Excitation and Tip Mass," *Journal of Sound and Vibration,* vol. 83, pp. 445-460, 1982.
[36] D. C. D. Oguamanam, "Free vibration of beams with finite mass rigid tip load and flexural-torsional coupling," *International Journal of Mechanical Sciences,* vol. 45, pp. 963-979, 2003.
[37] M. H. Mahdavi, A. Farshidianfar, M. Tahani, S. Mahdavi, and H. Dalir, "A more comprehensive modeling of atomic force microscope cantilever," *Ultramicroscopy,* vol. 109, pp. 54-60, 2008.
[38] M. Allen, H. Sumali, and D. Epp, "Piecewise-linear restoring force surfaces for semi-nonparametric identification of nonlinear systems," *Nonlinear Dynamics,* vol. 54, pp. 123-135, 2008.